Dye-Doped Polymer Nanoparticles for Flexible, Bulk Luminescent Solar Concentrators

By
Ron Rosenberg

Submitted to the
Department of Materials Science and Engineering
in Partial Fulfillment of the Requirements for the Degree of

Bachelor of Science
at the
Massachusetts Institute of Technology
June 2013

Signature of Author .....

Department of Materials Science and Engineering
May 7, 2013

Certified by .....

Professor Marc Baldo
Department of Electrical Engineering and Computer Science
Thesis Supervisor

Read by .....

Professor Silvija Gradecak
Department of Materials Science and Engineering
Thesis Reader

Accepted by .....

Professor Jeffery C. Grossman
Department of Materials Science and Engineering
Undergraduate Committee Chairman

Dye-Doped Polymer Nanoparticles for Flexible, Bulk Luminescent Solar Concentrators

By
Ron Rosenberg

Submitted to the
Department of Materials Science and Engineering
in Partial Fulfillment of the Requirements for the Degree of

Bachelor of Science
in Materials Science and Engineering

ABSTRACT

Bulk luminescent solar concentrators (LSC) cannot make use of Forster resonance energy transfer (FRET) due to necessarily low dye concentrations. In this thesis, we attempt to present a poly-vinylalcohol (PVA) waveguide containing dye-aggregate polystyrene nanospheres that enable FRET at concentrations below that required for the bulk LSC due to dye confinement. In the aqueous state, the maximum achieved energy transfer efficiency of the dye-doped nanoparticles was found to be 87% for 1wt%/1wt% doping of Coumarin 1 (C1) and Coumarin 6 (C6). In the solid state, however, energy transfer is lost, reducing to 32.8% and 20.1% respectively for the C1(1wt%)/C6(1wt%) and C1(0.5wt%)/C6(1wt%) iterations, respectively. Presumably, the dyes leach out of the polystyrene nanospheres and into the PVA waveguide upon water evaporation during drop casting.

Thesis Supervisor: Marc Baldo

Title: Professor of Electrical Engineering and Computer Science

ACKNOWLEDGMENTS

I owe much appreciation to Professor Marc Baldo, my principal investigator and supervisor, for welcoming me into the Soft Semiconductor Group. As a whole, the group provided a fun and challenging atmosphere that not only drove me to think critically, but also have fun in the process.

I specifically want to thank Phil Reusswig for being a fantastic direct supervisor. Throughout the process, Phil offered invaluable advice and support – from debugging test equipment to teaching me fundamental excitation physics. In addition, I valued Phil's persistence, patience, and attention to detail – traits that I hope to carry with me as I move forward in my graduate studies. I also want to thank Nick Thompson, Dan Congreve, and other members of the Soft Semiconductor Group who offered their informal advice and contagious enthusiasm.

TABLE OF CONTENTS

LIST OF FIGURES

20. **Figure 20**: Absorbance of solid state C1/C7 doped nanoparticles in PVA at different total wt% of dye for C1(1wt%)/C6(1wt%) model.

LIST OF TABLES

INTRODUCTION AND THEORY

A.) The need for a better $/W of solar energy

Solar photovoltaic (PV) energy has experienced exponential growth over the past two decades [1]. Most of this growth is due to the increased efficiencies and declining costs of solar technologies, the latter of which can be attributed to favorable economies of scale and manufacturing improvements [2]. In these ways, solar energy has become more and more cost-competitive with conventional fossil fuels – coming down from nearly $65 USD/Watt in 1975 to only $4 USD/Watt in 2011 [2],[3] as compared to $1 USD/Watt [2],[3] for conventional fossil fuels. Figure 1 below indicates the relative progress in cost reduction that solar modules have achieved up until present day.

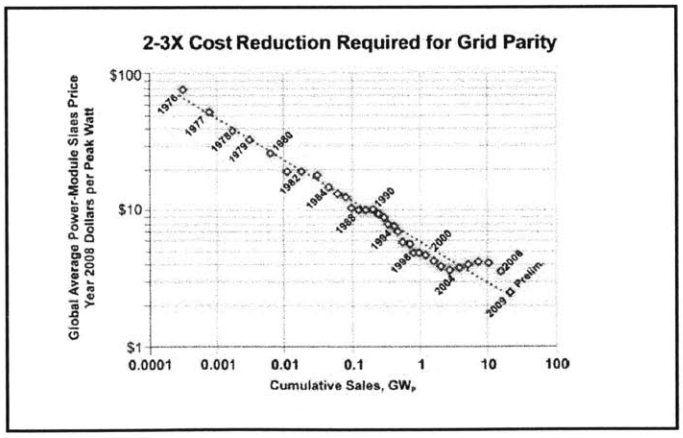

Figure 1: The global average module sales price in $/Wp in 2008 dollars.

At the current state, however, even when taking into account externalities associated with fossil fuel electricity generation, the levelized cost of solar electricity (PV,

thermal, or concentrated) remains at best double that of coal or natural gas [3]. Therefore, along with fundamental research in achieving higher conversion efficiencies, the biggest challenge for solar PV energy is the 2-3 times reduction in capital cost necessary to reach the grid parity with conventional fossil fuels [3],[4],[5].

B.) Solar concentrators

Solar concentration offers a solution to the high PV energy capital costs. While the total PV module cost includes installation cost, labor cost, etc – the largest cost remains that of the semiconducting material itself. According to the DOE, the cost of the PV module is 50% of the total cost of the installed system [6]. Solar concentrators address this issue by using a large, relatively inexpensive concentrator (often a glass mirror) that focuses light onto a small PV element. By minimizing the relative amount of PV material used, the overall cost decreases. To help quantify this relative cost reduction, the geometric gain, G, can be used. G measures the relative area occupied by the solar cell to that of the concentrator material [7].

$$G = \frac{A_{solar\ cell}}{A_{concentrator}} \tag{1.1}$$

G is an important metric for measuring the economic advantage of solar concentrators. As G increases, the relative cost of the PV is minimized and the cost of the concentrator material dominates [7]. Given that the concentrator material is cheaper than

that of the PV material, a larger G is favorable for a more cost-competitive solar concentrator.

A more accurate measure of the economic advantage of solar concentrators is the flux gain. The flux gain is essentially the geometric gain, but multiplied by the external quantum efficiency (ratio of photons in to photons out) of the concentrator [7]. In this way, the flux gain measures the relative increase in incidental flux that concentrators offer:

$$F = \eta_{EQE} * G \tag{1.2}$$

F is an important factor when calculating the $\$/W_{peak}$ of the solar concentrator. As evident in equation 1.3, as F increases, the $\$/W_{peak}$ of the PV system decreases, thereby making it more cost competitive [5],[7]:

$$\frac{\$}{W_p} = \frac{1}{solar\ flux} * \left(\frac{collector\ cost}{collector\ efficiency} + \frac{1}{F}\frac{PV\ cost}{PV\ efficiency}\right) + maintenance \tag{1.3}$$

Despite the theoretical cost and efficiency advantages of concentrated solar power, there are numerous drawbacks. First and foremost, in order to achieve a high G and high optical intensities, the concentrator must be nearly normal to the sun. Because of this limitation, concentration systems need to follow the sun's trajectory in the sky – thereby requiring expensive one to two-axis tracking systems. Notably, these tracking systems are not only highly capitally intensive to deploy, but also expensive to maintain. In addition, because the tracking concentrators only concentrate direct sunlight, they can only perform well on sunny days or in sunny areas – when the sun is directly exposed. For this

reason, solar concentrating systems are typically only found in the Southwest United States where sunny days are plentiful [8].

Another issue with traditional solar concentrators arises from the high solar flux that is incident on the PV cells. Because Ohmic losses scale quadratically with the intensity of incident sunlight, solar cells in concentrated PV systems need expensive cooling systems to avoid degraded performance over time [9]. The dual need of tracking and cooling systems for solar concentrators greatly increases their costs, thus making them less competitive in the market. Therefore, there exists a significant need for an inexpensive solar concentrator that can help propel solar energy forward in the global market.

C.) Luminescent solar concentrators

i.) Basic principle of operation

The luminescent solar concentrator (LSC) was introduced in 1976 by Weber and Lambe [10],[11] as a design alternative that could achieve high optical concentration without the need of expensive tracking and cooling systems [5]. The simplest version of an LSC is a glass or plastic substrate doped with an organic dye. Notably, however, LSCs today can consist of a range of hosts and chromophores – from organic luminescent dyes to quantum dots, and even semiconducting polymers [10],[12],[13],[14],[15]. In all LSC manifestations, incident photons are absorbed by the flourophores and fluorescently re-emitted at a red-shifted wavelength [15]. Emitted photons at angles less than the critical

angle of total internal reflection at the LSC/air interface then travel through the waveguide to the edges of the concentrator, where PV cells are situated. Finally, the PV cells convert the incidental radiation to electricity. A basic schematic of a typical single-dye LSC can be found in Figure 2 below:

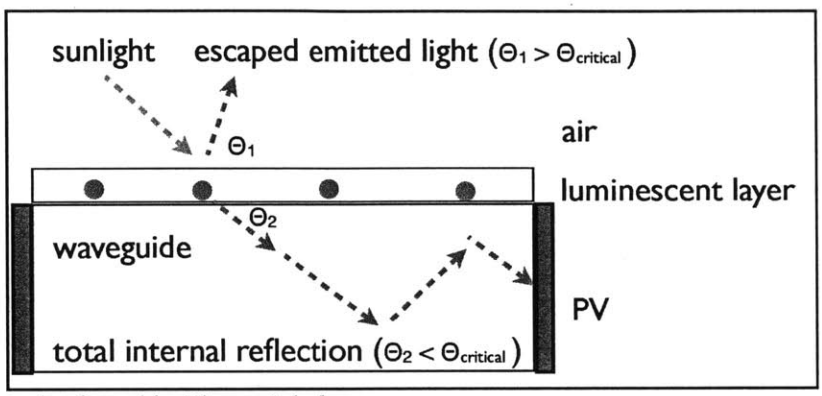

Figure 2: A schematic describing LSC operation. Sunlight (green arrow) enters the LSC and interacts with a fluorescent species (red dots), which then emits light radially (red line). Light greater than the critical angle for internal reflection is trapped into the waveguide and directed to the PV modules at the LSC sides.

ii.) LSC advantages

LSCs offer numerous advantageous over traditional solar concentrators. First and foremost, LSCs do not require expensive tracking mechanisms. Due to the isotropic absorption of the organic molecules in the waveguide, LSCs can concentrate both direct and diffuse sunlight [7], [15], [16]. Therefore, the LSCs can operate at any angle relative to the sun and are less affected by cloudy days.

Second, LSCs also do not require any cooling mechanisms. This is because the dyes in the LSCs can be chosen to convert the incident solar spectrum into "down-

shifted" or "red-shifted" monochromatic light matched to the bandgap energy of the PV cell [17]. In this way, the PV cell achieves higher external quantum efficiency by reducing thermal losses associated with higher energy photons relaxing to lower energy states [17]. Notably, in practice, the energy of the emitted photons from the dye molecule is slightly greater than that of the bandgap to ensure the highest conversion efficiency possible [4].

LSCs also offer the advantages of inexpensive fabrication [7]. LSCs can benefit from well-known and inexpensive polymer/glass casting or polymerization processes – such as spin casting, drop casting, molding, or cross linking [7]. In addition, besides the PV cell, LSCs use relatively cheap and abundant materials. This is especially important because many solar PV technologies require either expensive materials or rare earth materials – like Cadmium or Indium – or materials that require intensive processing and purification – like silicon [18].

Finally, LSCs can be used for building integrated photovoltaic (BIPV) applications [19]. Because LSCs consist of a transparent waveguide with the PV modules only at the sides, they are favorable candidates as solar windows. In addition, due to the flexibility of polymer-based LSCs, they can be integrated into curved building surfaces. Cylindrical LSCs have also been prototyped [20], underscoring the potential application of LSCs towards interesting building architectures.

iv.) LSC physics and operational losses

As with any real system, there are numerous operational losses that make it

perform worse than the theoretical maximum. For an LSC specifically, the realized flux gains are far smaller than the thermodynamic theoretical maximum predicted by Yablonovitch et al [21]. The overall external quantum efficiency (EQE) of an LSC, excluding that of the PV cell, can be described by the product of the efficiencies of each step a photon takes upon entering the LSC until reaching the PV cell. Each step in the photon pathway can also be thought of as a source of operational loss [7], and consequentially, an opportunity for design and innovation.

For a single-chromophore LSC, those steps can be summarized as: (1) absorption of sunlight into LSC (2) absorption of light by luminescent species (3) photoluminescence of light by the luminescent species (4) trapping of emitted light (5) total internal reflection of emitted light into waveguide (6) transmission and total internal reflection through waveguide (7) absorption by other dye molecules:

$$\eta_{LSC} = (1 - R) * \eta_{abs} * \eta_{PL} * \eta_{trap} * \eta_{trans} * \eta_{TIR} * \left(1 - \eta_{self}\right) * \eta_{abs} \quad (1.4)$$

Where R is the reflection coefficient of the LSC material, η_{abs} is the absorption efficiency of the photoluminescent species; η_{PL} is the photoluminescence efficiency of the photoluminescent species; η_{trap} is the trapping efficiency of escaped light; η_{TIR} is the efficiency of total internal reflection in the waveguide, and η_{self} is the self-absorption efficiency of the photoluminescent species. Below is a description of the physics behind the most important loss mechanisms and their implications towards material and design choices for optimal performance.

In the first step of the pathway, some of the radiation incident on the LSC will be lost reflected, as show in in Figure 3 [22].

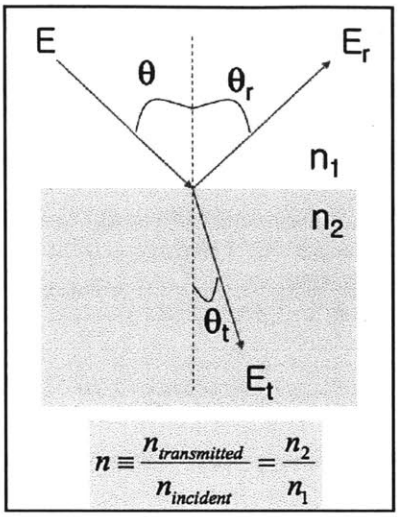

Figure 3: Electromagnetic radiation at a boundary between two different materials with different refractive indices. Incident radiation in a medium 1 of refractive index n_1 comes in at angle θ_i and is reflected at a θ_r. Transmitted electromagnetic radiation propagates through medium 2 of refractive index n_2 and angle θ_t.

The percentage of reflected and transmitted sunlight can be determined by using the square of Fresnel reflection coefficient (for TE polarized light) [23], which is given by equation (1.5):

$$R = \left(\frac{cos\theta - \sqrt{n^2 - sin^2\theta}}{cos\theta + \sqrt{n^2 - sin^2\theta}}\right)^2 \tag{1.5}$$

Where θ is the angle of incidence, n is the ratio of the refractive index of air to that of the transparent waveguide of the LSC [19]. In order to minimize this operational loss via reflection, it is favorable to choose waveguide materials that have a high refractive index (~1.5 to 1.6) and do not scatter light. Fortunately, there are many high-index transparent materials that are inexpensive and commercially available – such as glass and high-index polymers like PMMA or PVA.

Another important step happens afterwards, when light that is transmitted through the LSC-air interface is absorbed by the photoluminescent species. When the dye absorbs the photon, it gains energy and enters and excited state, as shown in Figure 4 below:

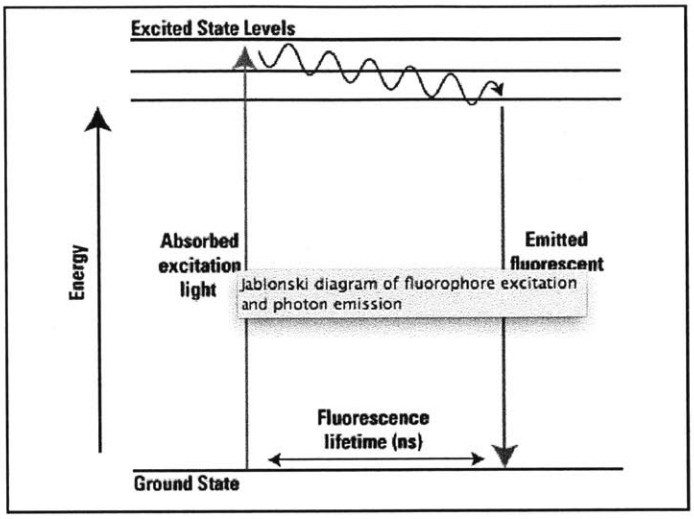

Figure 4: A typical energy level diagram of a fluorescent molecule. Incident photons are absorbed by ground state electrons, which subsequently jump to excited states. During the time of the jump, some of the energy is dissipated through molecular collisions (released as heat) or through energy transfer to nearby molecules. Upon relaxation to the ground state, the remaining energy is released in the form of an emitted photon.

From then on there are two ways for the system to relax down to the ground state: releasing heat (phonons) or emitting radiation (photons) [23]. Both relaxation modes present different losses in the LSC.

The first loss is dependent on the photoluminescence (PL) efficiency of the dye – that is, the ratio of emitted photons to absorbed photons. If the chromophore is not PL efficient, most of the energy will be released as heat, which cannot be used for electricity generation later. Optimal LSC designs, therefore, employ highly PL efficient dyes. Fortunately, many commercially available dyes have near unity PL efficiency especially in

the visible spectrum, such as the Coumarin family and the Rhodamine family. Unfortunately, however, there are not many highly efficient dyes that can emit in the near-infrared (n-IR), the optimal wavelength for conventional silicon solar cells. For this reason, quantum dots have gotten increased interest since they are both highly PL efficient and can be tuned in size to emit in the n-IR [24]. Regardless of the dye choice, however, the dye PL efficiency is dependent on the temperature and the chemical environment [24],[25], so efficient LSCs must ensure that the dyes remain highly PL efficient upon incorporation into the LSC.

Even if the chromophore is highly PL efficient, there is a second loss mechanism associated with photon emission. As shown in Figure 5 most dyes have a non-negligible energy drop between the peak absorption wavelength and emission wavelength of the dye. The difference in wavelength between the two peaks is called the Stokes shift. Therefore, materials with a high Stokes shift will suffer from a high loss associated with down-conversion. But, as discussed later, higher Stokes shifts are also favorable due to decreased self-absorption of the dye.

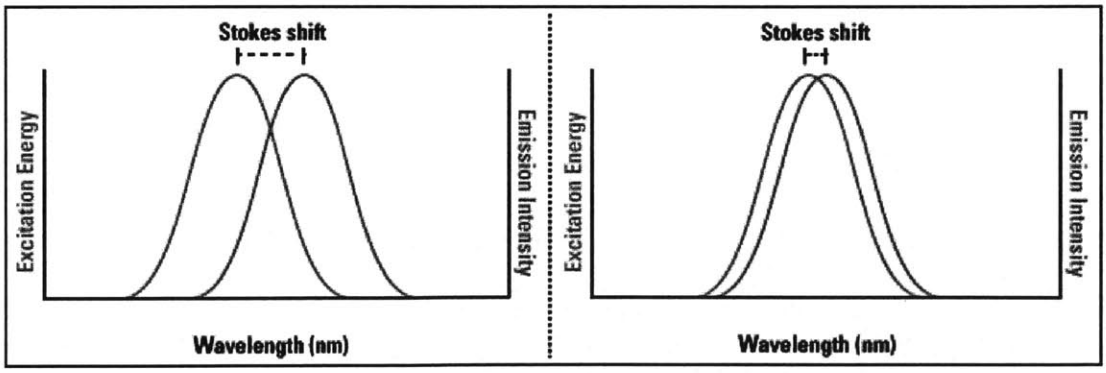

Figure 5: The Stokes shift is the difference (in wavelength) between the positions of the absorption band (blue) and emission band (red) maxima. According to the figure, the dye on the left has a larger Stokes' shift

than the dye on the right.

In the next step of the photon path, photons are emitted by the excited chromophore. Because most LSC designs employ randomly oriented dyes, they collectively photoluminesce in all directions [7]. To that end, energy is lost because a fraction of the emitted light escapes the waveguide because it is at an angle larger than the critical angle for total internal reflection [7]. The critical angle for total internal reflection is given by equation 1.6:

$$\theta_c = \arcsin\left(\frac{n_1}{n_{WG}}\right) \tag{1.6}$$

Where n_1 is the refractive index of air and n_{WG} is the refractive index of the waveguide material. The solid angle where light is trapped is called the "trap cone" whereas the solid angle where light escapes is called the "escape cone" [26]. In order to decrease the critical angle, and thereby decrease the "escape cone" of light that is not trapped in the waveguide, it is once again beneficial to have a highly refractive material. This is reflected also in the trapping efficiency of the LSC, which is:

$$\eta_{trap} = \sqrt{1 - \frac{1}{{n_{WG}}^2}} \tag{1.7}$$

Trapped photons then travel through the waveguide to the PV cells at the sides, leading to transport losses due to interactions with the waveguide material and other dye molecules. In order to reduce losses by the waveguide, the material should have low-scattering losses and not absorb in the characteristic emitted wavelength of the photoluminescent species. A recent study by Debije et al [27] showed that four common high-index transparent materials – Quartz, Polycarbonate, PMMA, and glass – all have

similar transmission characteristics for a Lumogen-Red dye based system. While this is only for one type of LSC system, the study suggests that most common high-index transparent materials will perform similarly, so this is less of a design constraint.

On the other hand, emitted photons interacting with other dye molecules poses one of the biggest operational losses of typical LSCs: self-absorption losses. Although most dyes have a Stokes shift, there is still often a large overlap between the absorption and emission spectrum. This results in a significant absorption of the emitted light of the chromophore, given by the finite overlapping area between spectra, marked in purple in Figure 6 below:

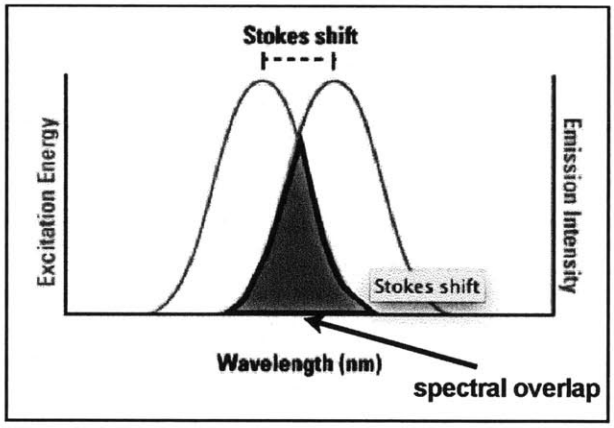

Figure 6: The spectral overlap (purple area) between the absorption (blue) and emission (red) spectrum of a typical dye molecule.

Self-absorption losses are particularly harmful for LSCs because it effectively limits the maximal G possible. As G increases, the "optical path" of the photon increases, therefore there is a greater likelihood of self-absorption events. This concept is

demonstrated by a numerical model presented by Currie, who modeled the effect of self-absorption on the fraction of intensity reaching the PV versus the geometric gain [26]. As evident from Figure 7 below, self-absorption causes light reaching the PV to decrease exponentially with increasing G [26].

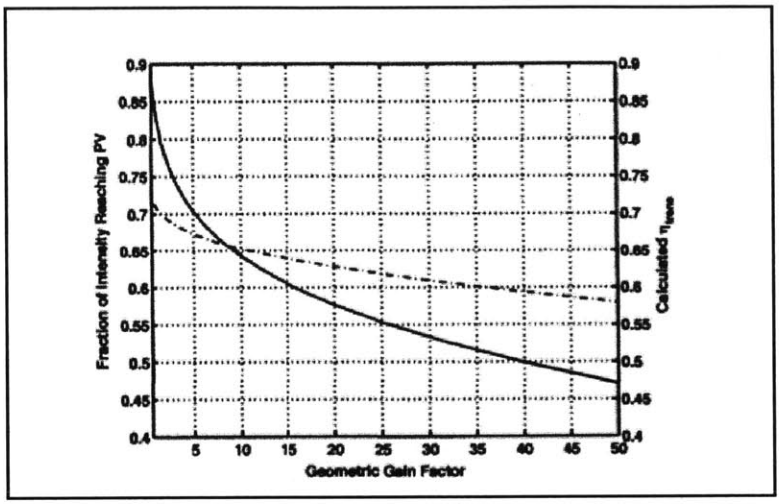

Figure 7: The fraction of incident radiation (solid line) reaching the PV element as a function of geometric gain (G) – as compared to experimental data (dashed line).

In this way, the efficiency of the LSC decreases exponentially due to self-absorption since every re-absorption event leads to a new generation of PL and trapping losses [7]. For a given number of re-absorption events, m, the efficiency of the LSC can be approximated as:

$$\eta_{LSC} \sim (\eta_{trap} * \eta_{PL})^m \tag{1.8}$$

For this reason, it is highly favorable to choose materials with a high Stokes' shift, such as quantum dots, so as to reduce the number of re-absorption events. Of course, this

comes with the tradeoff of a reduced absorption of the solar spectrum. Regardless, the dominance of these self-absorption losses has limited the G of LSCs and thereby negatively impacts their commercialization [26]. In order to achieve higher G's and ultimately commercialize LSCs, it is necessary to design LSCs that minimize self-absorption.

v.) Multi-dye LSCs

LSCs that make use of multiple dyes simultaneously increase solar spectrum absorption and minimize self-absorption [28]. There are numerous types of multi-dye LSC designs, including multi-dye plates [29], tandem thin-film LSCs [5],[29], and multi-chromophore conjugated polymers [30]. The first advantage of this type of LSC stems from the fact that a single dye absorbs a small fraction of the solar spectrum [26]; therefore, a system with multiple dyes will have a wider absorption [29], an increased η_{abs} of the LSC. Meanwhile, self-absorption losses are addressed through a process called Forster Resonance Energy Transfer (FRET) between the two dyes.

FRET is a non-radiative energy transfer process between an excited electron in a donor molecule (D) to an acceptor molecule (A) [31]. With FRET, a donor molecule absorbs the incident solar spectrum and then transfers energy to an acceptor, which then emits radiation. In this way, the Stokes shift is effectively increased since the absorption spectrum of D and emission spectrum of A are farther spaced than that of the single dye. As shown in in Figure 8, this increased Stokes shift leads to decreased self-absorption losses because there is less of an overlap between the absorption spectrum of D and

emission spectrum of A. Notably, however, this assumes that energy transfer is 100% efficient, with no emission of the donor (D).

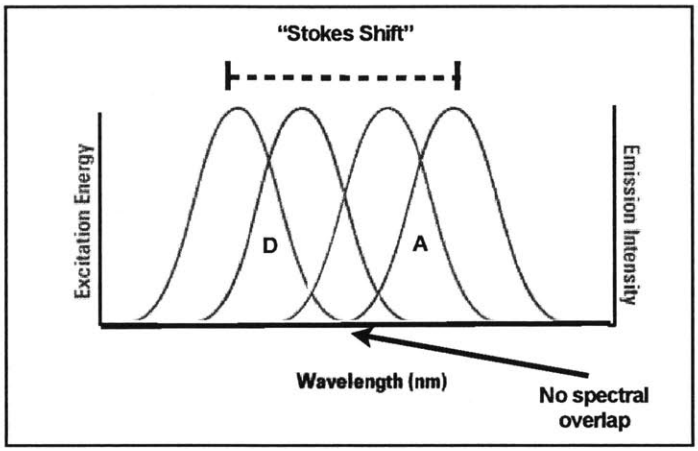

Figure 8: The effective total "Stokes Shift" of a multi-dye system undergoing energy transfer. The spectral overlap now becomes that between the absorption spectrum (blue) of the donor (D) and emission spectrum (red) of the absorber (A).

The electronic excitation transfer arises from dipole-dipole interactions between the donor and acceptor, and occurs without the emission of emission of light. The interaction depends on the following criteria (1) spectral overlap between the emission spectrum of the donor and the absorption spectrum of the acceptor (2) dipole alignment, and (3) spacing between D and A. This spacing is called the Forster radius, R_0, given by equation 1.9:

$$R_0{}^6 = 8.8 * 10^{-28} * \varphi_D * \kappa^2 * n^{-4} * J(\lambda) \qquad (1.9)$$

Where φ_D is the fluorescent quantum yield of the donor in the absence of the acceptor, κ is an orientation factor depending on dipole-dipole interaction, n is the refractive index, and $J(\lambda)$ is the spectral overlap between the absorption and emission

peak of the acceptor and donor, respectively. In addition, it is important to note that the Forster radius scales to the sixth power, underlining the sensitivity of the energy transfer process to the distance between D and A.

The FRET efficiency can be quantified in numerous ways. The first way takes into account the respective distance, R, that D and A are spaced from each other and compares it to the Forster radius, R_0. As evident by the equation 1.10 below, when R is equal to R_0 the energy transfer efficiency is equal to only 50%.

$$\eta_{FRET} = \frac{{R_0}^6}{{R_0}^6 + R^6} \tag{1.10}$$

It is also possible to solve for the energy transfer efficiency graphically using photoluminescence (PL) data, which is the PL emission spectrum of a phosphor upon excitation. The FRET efficiency of the multi-dye system can be measured as the integral of the normalized PL spectrum associated with the donor (where the donor has appreciable absorption) and dividing it by that of the acceptor [28]. In the case of full energy transfer, the total integral of the emission spectrum should be 100% comprised of the acceptor emission.

viii.) Thin film and bulk film multi-dye LSCs

LSCs that make use of FRET must strike a delicate balance. While FRET relies upon high enough concentrations to ensure close proximity of D to A within the Forster

radius, higher concentrations lead to higher self-absorption losses. This is because for a given optical path length, higher concentrations have a larger number of dye molecules along that path – and hence, more opportunities for self-absorption events. Optimal design of an LSC, therefore, makes use of FRET without self-absorption losses.

Thin film tandem (TFT) LSCs overcome this restriction by having concentrations at or above the concentration threshold for FRET, but a thin enough film that minimizes self-absorption of the dye. TFT LSCs are usually manufactured through spin casting or thermal evaporation of the dyes onto an undoped glass substrate, leaving a thin layer on the order of 150-1000 microns [32]. Light that is emitted into the undoped layer and trapped via total internal reflection therefore has a much lower chance of being reabsorbed [32]. With such small thicknesses, thin film tandem LSCs can make use of FRET without being deterred by self-absorption losses.

But once the thickness of these tandem LSCs increases on the order of millimeters, self-absorption becomes a serious problem. As shown in Figure 9, increasing the thickness leads to a higher likelihood of dye quenching. FRET efficiency therefore greatly decreases due to the self-quenching of absorber emission:

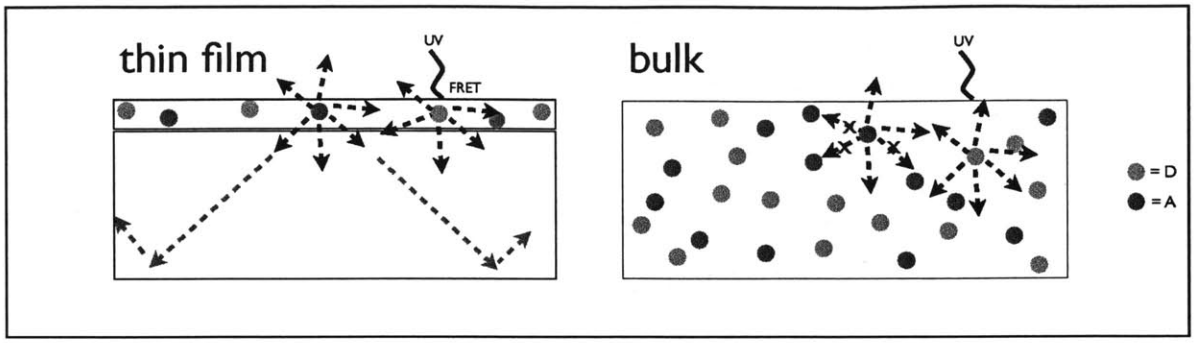

Figure 9: On the left is a typical thin-film multi-dye LSC that makes use of energy transfer. Upon increasing the thickness of the thin-film LSC, self-absorption losses become dominant, leading to decreased energy transfer efficiency. The only way to reduce self-absorption losses is to decrease the concentration, and therefore space the particles farther away than the Forster radius. Bulk multi-dye LSCs therefore cannot make use of energy transfer due to the necessarily low concentrations to avoid self-asborption losses.

To that end, there is a need for a bulk multi-dye LSC that can make use of energy transfer without being hindered by self-absorption losses. This thesis addresses this design challenge using dye-aggregates. Dye aggregates have been a popular approach specifically in biological sensing applications [33],[34]. In these cases, nanoparticles – popularly silica nanoparticles [34] – are doped with either one dye or multiple dyes that can undergo energy transfer. These nanoparticles are ideal for *in-vivo* imaging and other bio-photonic applications due to their fluorescent properties, biocompatibility, and easy surface modification [34].

But beyond biological applications, dye-doped aggregates have immense potential for use in LSCs. A bulk LSC that incorporates dye-doped nanoparticles would have a high enough *local* concentration inside the nanoparticle conducive to FRET but a "low" enough *overall* concentration for minimal self-absorption. In addition, a dye-doped bulk LSC would offer the advantage of flexibility since it would be trivial to incorporate the

aggregates into a flexible polymer like PVA, PMMA, or PLGA – as opposed to a rigid borate glass. A schematic of a dye-aggregate based LSC is found below:

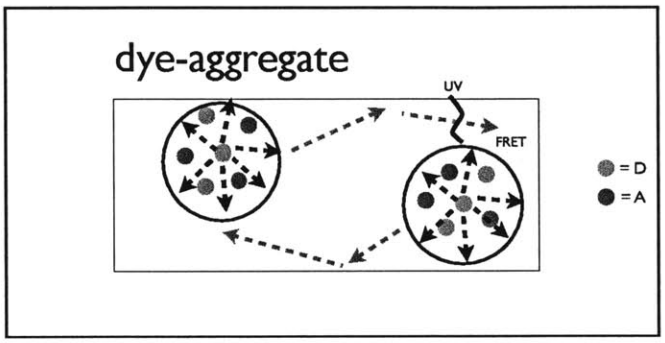

Figure 10: A dye-aggregate multi-dye LSC confines the donor (green dots) and acceptor (red dots) into a nanospheres. By achieving local dye concentration, energy transfer is possible without the problem of self-absorption losses.

vii.) Achieving dye-confinement in nanospheres: swelling-evaporation

The swelling-evaporation technique is one general method of localizing the dyes in nanospheres [35]. The swelling approach depends on a diffusive driving force that arises from differences in solubility between the host solvent of the nanoparticles and the nanoparticle themselves. Given that luminescent dyes are typically hydrophobic, water is often chosen as the host solvent of the nanoparticles, since it is selectively poor for the dyes [36]. The nanoparticles themselves are often hydrophobic ceramic or polymer nanospheres, such as Silica, PLGA, or PMMA [36], [33], [34]. Meanwhile, the dye solvent is typically chosen to have poor solubility in the host solvent of the nanoparticles, as well as a high volatility in low boiling point [36]. THF, Chloroform and DCM are all solvents that meet the above criteria.

In the first step of the process, the dyes were dissolved in the aforementioned solvents. Then, the dye solution was added to an aqueous solution of nanoparticles in water [37]. In the next step, continuous rotary evaporation of the dye solvent leads to the dye molecules preferentially diffusing into the nanoparticles, in which they have a higher solubility than in water. Once the dye solvent is completely baked off, the dye molecules are successfully incorporated into the microsphere interiors. A diagram of the solvent-evaporation process using polystyrene nanospheres is found below:

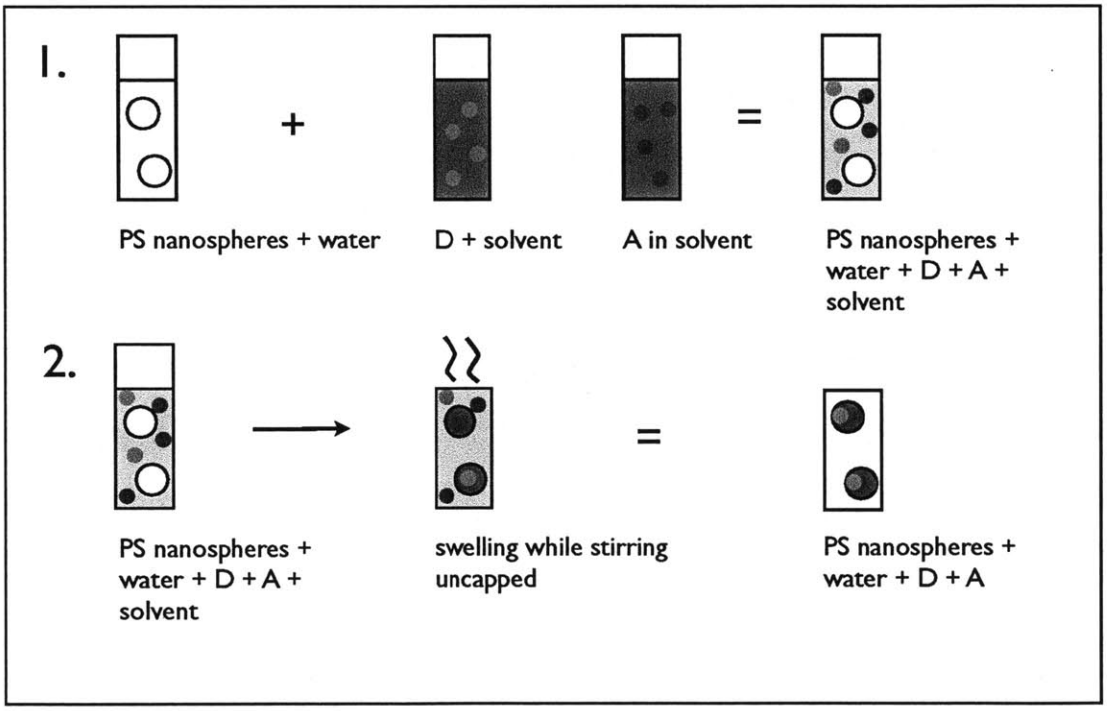

Figure 11: In the first step of the process, the dyes are dissolved in the aforementioned solvents. Then, the dye solution is added to an aqueous solution of nanoparticles in water [31]. In the next step, continuous rotary evaporation of the dye solvent leads to the dye molecules preferentially diffusing into the nanoparticles, in which they have a higher solubility than in water. Once the dye solvent is completely baked off, the dye molecules are successfully incorporated into the microsphere interiors.

EXPERIMENTAL

A.) Preparation of the multi-dye LSC

i.) Dissolving the dyes

We examined two emissive dyes: 7-Diethylamino-4-methylcoumarin (Coumarin 1, Sigma-Aldrich, 99%) and 3-(2-Benzothiazolyl)-7-(diethylamino)coumarin (Coumarin 6, Sigma-Adlrich, 98%). The Coumarin dye family is used for a wide variety of applications – from anti-inflammation to dye sensitized solar cells [38]. They are specifically of interest due to their high absorption cross-sections and fluorescence quantum yield [39]. They are also model dyes for a multi-dye LSC making use of energy transfer since they have a high spectral overlap.

The dyes were dissolved in Dichloromethane (DCM) at a concentration of 8mg/mL. The solutions were placed on a hotplate at 90C and left to stir overnight for 12 hours to achieve a completely uniform solution. Once the dyes were completely dissolved they were filtered using a .45um PVDF filter.

Notably, DCM was chosen as the final solvent after a few iterations that included THF, Chloroform, and Acetone. In the end, DCM was the only dye that best supported both the complete dissolution of Coumarin 1 (C1) and Coumarin 6 (C6), as well as the swelling of the nanoparticles in later stages.

ii.) Making the dye-doped nanoparticles via swelling-evaporation

We used 25 nm polystyrene (PS) nanoparticles (NPs, Phosphorex). The PS NPs were purchased suspended in a 3.2 wt% aqueous solution that consisted of de-ionized water, a small amount of surfactant, and 2mM of sodium azide as an anti-microbial agent. 25nm NPs were chosen specifically because we wanted sub-visible wavelength nanoparticles that would not scatter light once incorporated into the LSC. In addition, we thought that the higher surface area to volume ratio of the smaller nanoparticles would prove more favorable for dye diffusion into the NPs later on during the dye-doping process.

The first iteration consisted of a C1(1wt%)/C6(1wt%) dye doping ratio in the nanoparticles. This dye-doping weight percentage was chosen since it is high enough for energy transfer, but low enough to avoid concentration quenching. To that end, 40uL of the each dye solution was added to 1mL of NPs. Solutions were made of just C1 in nanoparticles, just C6 in nanoparticles, and finally C1/C6 in nanoparticles. The solutions were then stirred for 10 minutes capped to ensure that the dye solution mixed evenly around the nanoparticles. Subsequently, the solutions were stirred uncapped overnight to allow for the complete evaporation of the DCM. Once the dye-doped nanoparticle solutions were ready, they were filtered with a .2um PVDF filter to remove any dye aggregates that may have formed in solution.

The second iteration consisted of a C1(0.5 wt%)/C6(2 wt%) dye doping ratio. To that end, all steps of the process were the same, but we added 20uL of C1 and 80uL of C6 instead of 40uL.

For PL measurements, all nanoparticle solutions were diluted 1000 times in water. At such concentrations, the only way energy transfer could occur was if the donor and acceptor molecules were localized together in the nanoparticles, because such dilutions

would space the free molecules farther than the Forster radius. In addition, this high dilution was favorable because it allowed for accurate PL measurements, uncompromised by high levels of concentration quenching. Finally, these solutions were compared to control solutions of C1 and C6 in DCM at 1000 times dilution. Meanwhile, solutions for absorbance measurements were diluted 40 times in either water or DCM for the NPs or the dye controls, respectively. All solutions that contained DCM were thoroughly wrapped in Teflon tape, due to the extreme volatility of DCM.

iii.) Incorporating the dye-doped nanoparticles in the solid-state LSC

To cast the nanoparticles into a solid-state waveguide, Polyvinyl-alcohol (Mowiol® 4-88, Sigma-Aldrich, M_w ~31,000) was chosen as the matrix material. First and foremost, PVA is water soluble, allowing the addition of aqueous nanoparticle solution without phase separation. Upon water evaporation, PVA also does not readily phase separate with PS. Importantly, PVA's refractive index is 1.52-1.55, nearly matching that of PS, [41] which is 1.59 [40]. Therefore, scattering in the LSC could be minimized by index matching, allowing for a transparent LSC. PVA also offers excellent mechanical and chemical properties – allowing it to be both withstand tears and resist deformation even at high temperatures [42].

PVA was dissolved at a concentration of .12g/mL and subsequently heated at 90C for 4 hours. The effect of reabsorption was studied by making subsequent solutions of .01wt%, .001wt% and .0001wt% dye in nanoparticles in PVA for both iterations of C1/C6 doped nanoparticles. The PVA-dye solutions were then left capped and spinning overnight for complete mixing. 400uL of these solutions were then drop-casted onto a

1cm x 1cm x 1mm clean glass slide (Eerie scientific, n=1.5) and left to dry overnight. In theory, if the nanoparticles were efficiently doped, their PL emission spectrum should not change at successive dilutions.

B.) Analysis and instrumentation

PL emission spectra were recorded using a fluorescence spectrometer by exciting the samples at with a ThorLabs M365L2 – UV 365 LED light source. While PL integration times varied between solution data and solid-state data, integration times were remained constant for the respective iterations and for the DCM and Nanoparticle data sets. Rather than using a filter, the laser contribution was first attempted to be removed in MATLAB by finding a least squares fit to the laser-only spectrum and subtracting that from the emission spectra of the samples. However, due to the lack of symmetry of the emission spectrum of the LED light source, this did not yield accurate results. The second attempt at removing the light source was simply filtering out all emission below 400 nm, which includes only the laser since Cl's emission band edge is at 400nm [43].

The PL setup consisted of a large ThorLabs – LA1131ML convex lens that focused the LED light onto the sample holder. The optical fiber was placed at a 30-degree angle from the LED beam but normal to the sample in order to measure only the PL reflected off the face of the sample, rather than the sides, which correspond to a longer optical path length. By establishing a shorter path length that corresponds to excitation near the edge facing the detector, the effects of self-absorption on the PL emission are minimized for the solid-state samples. A picture of the setup is below:

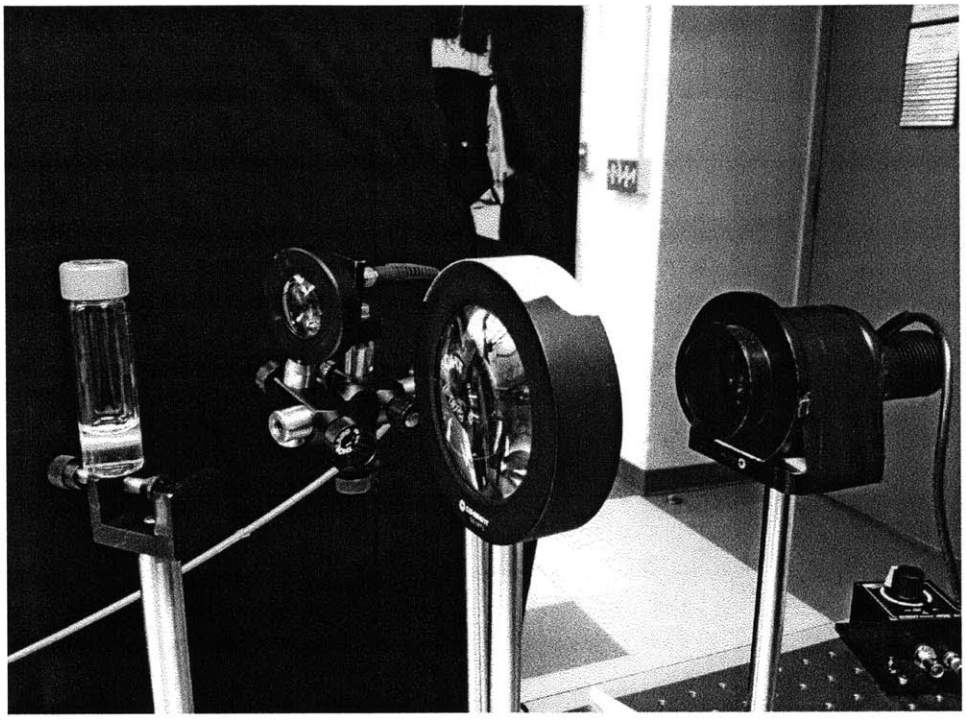

Figure 12: A picture of the PL setup. The sample is oriented at 30 degrees to the LED beam and the optical fiber (red wire). The LED beam is focused onto the sample with a lens, situated in the middle. The power of the LED was controlled by the control on the bottom left. For each experiment the power was at the maximum.

Absorption measurements of the nanoparticle and dye solutions were taken using a Perkin Elmer Lambda 950 UV/VIS Spectrophotometer. All solid-state absorption measurements were obtained using an Aquila Spectrophotometer.

RESULTS AND DISCUSSION

A.) Model verification

Before analyzing the nanoparticles, it was essential characterize the C1/C6 system to verify if it was indeed a valid system that could make use of energy transfer. Figure 13 below shows the PL emission and absorption spectra of C1 and C6 in DCM.

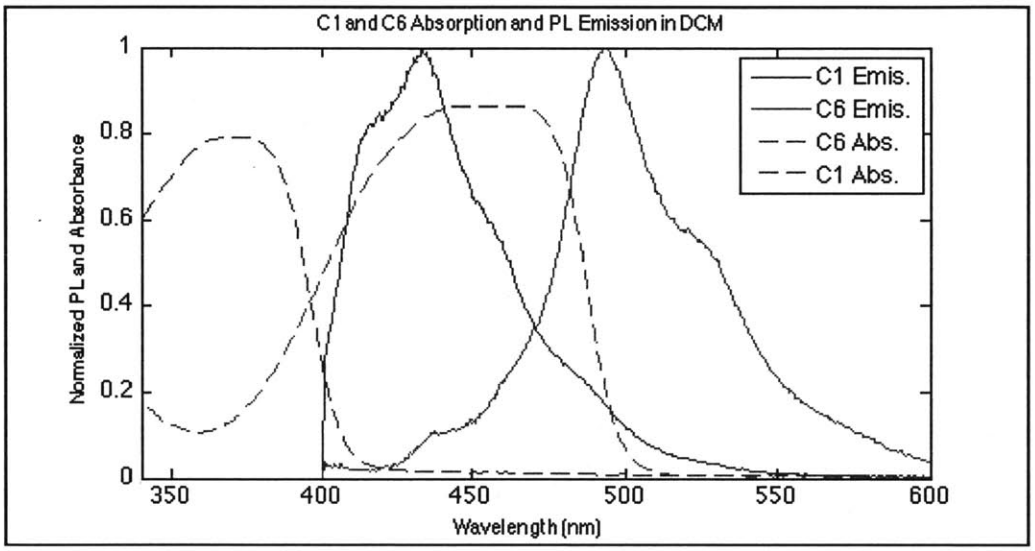

Figure 13: PL emission and absorbance of C1 and C6.

For a system to make use of energy transfer, the emission spectra of the donor and the absorption spectrum of the acceptor should overlap. As show in Figure 13, the emission spectrum of C1 and absorption spectrum of C6 indeed overlaps with a significant spectral overlap that spans 138 nm, more than the entirety of the C1 emission

spectrum. Therefore, the C1/C6 model was a valid model that can make use of energy transfer.

Here, the peak absorption and emission wavelengths of C1 and C6 can be identified. C1 has an absorption peak at 371 nm and emission peak at 433 nm, resulting in a Stokes shift of 62 nm. Meanwhile, C6 has an absorption peak at 451 nm and peak emission at 493 nm, resulting in a Stokes shift of 42 nm. With these absorption and emission peaks in mind, it is now possible to determine the doping efficiency and relative PL efficiency of the dyes in the nanoparticles.

i.) Energy transfer efficiency of C1/C6 dye-doped nanoparticles in solution

Once the swelling-evaporation process was completed, we wanted to verify that we indeed had dye aggregates and that the dyes were undergoing energy transfer. To that end, absorption measurements indicated the presence of the dyes in the nanoparticles, whereas PL emission measurements indicated whether or not energy transfer was occurring. Given that the PL solutions were diluted 1000x, the only way energy transfer would occur is if there was a dye-aggregate, because such dilutions spaced the molecules farther apart than the Forster radius. Figure 14 shows the PL and Absorption spectrum of C1, C6, and C1/C6 doped nanoparticles (from top to bottom) of the 1wt%/1wt% iteration (left) and the 0.5wt%/2wt% iteration (right).

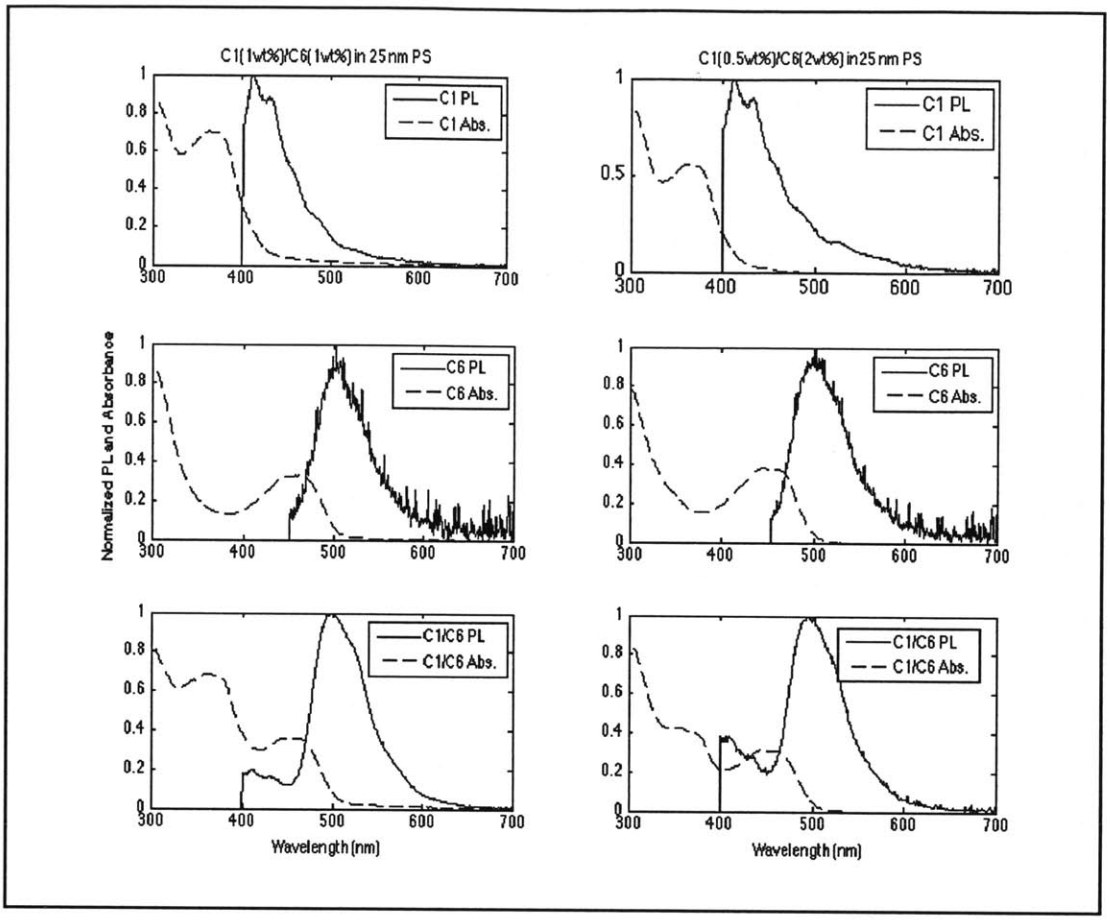

Figure 14: Normalized PL and absorbance spectra of the C1, C6, and C1/C6 doped nanoparticles in aqueous solution.

In the bottom row of Figure 14, the two distinct absorption peaks consistent with C1 and C6 indicate that both dyes are present in the nanoparticles. Meanwhile, the PL spectrum indicates that both iterations of the nanoparticles made use of energy transfer, because the PL spectrum has a dominant peak at 496 nm – consistent with the emission peak of the acceptor, C6. Had energy transfer not been occurring, there would have been two distinct peaks matching the relative magnitudes of the C1 and C6 emission in the first and second rows, which represent nanoparticles doped with C1 and C6 only, respectively.

Because the integration times for the PL emission measurements were the same for each set NP solutions, the energy transfer efficiency of the C1/C6 doped nanoparticles could be calculated using the ratio of peak PL emission at 433 nm for the C1/C6 doped nanoparticles with respect to that for the C1 doped nanoparticles:

$$ETE = 1 - \frac{PL_{433,C1/C6}}{PL_{433,C1}}$$

For C1/C6 doped nanoparticles, the C1(1wt%)/C6(1wt%) iteration had an energy transfer efficiency of 87%. Meanwhile, the C1(0.5wt%)/C6(2wt%) iteration had an energy transfer efficiency of 76.7%. This suggests that the C1 and C6 molecules are not only successfully incorporated into the nanospheres, but also that they undergo energy transfer at a high rate.

The reason that the second iteration had a lower energy transfer efficiency is likely due to the relatively smaller number of donor molecules inside the nanoparticles with respect to the first iteration. This can be seen from the 47% reduction in the C1 absorption peak from the first to second iteration, which is consistent with the 50% smaller C1 doping percentage in the second iteration. With fewer donor molecules present in the nanoparticles, energy transfer is less likely, and therefore the energy transfer efficiency is decreased.

B.) PL efficiency of C1 and C6 in nanoparticles

Subsequently, we wanted to determine the PL efficiency of the dyes inside the nanoparticles. In order to achieve a highly efficient LSC with a high quantum yield, the PL efficiency of the dyes needed to be high. Therefore, calculating the PL efficiency of the dyes was an important step in determining the prospect of this system for future LSCs.

The PL efficiency of the dye can be found by first determining the PL efficiency of the dye-doped nanoparticles with respect to a control. Here, the control consisted of DCM with the same amount of dye that was added prior to the solvent-evaporation procedure for each iteration. The PL efficiency of the dye-doped nanoparticle with respect to this control is therefore dependent on the number of dye molecules that make it into the polystyrene, as well as the PL efficiency in the polystyrene environment. Therefore, the PL efficiency of the dyes in the nanoparticles can be summarized as:

$$\eta_{PL,NP} = \eta_{uptake} * \eta_{PL,dye}$$

Where η_{uptake} is the fraction of dye molecules that successfully diffuse into the nanoparticles, $\eta_{PL,dye}$ is the dye PL efficiency inside the nanoparticle and $\eta_{PL,NP}$ is the resultant total PL efficiency of the dye-doped nanoparticle. Ideally, if the solvent-evaporation approach were 100% effective and the dye had a 100% PL efficiency inside the polystyrene, the PL spectrum of the dye doped nanoparticle would match that of the control.

In order to determine the PL efficiency of the dye-doped nanoparticles, the PL nanoparticle spectra were collected against the DCM control. Figure 15 shows a summary of this data:

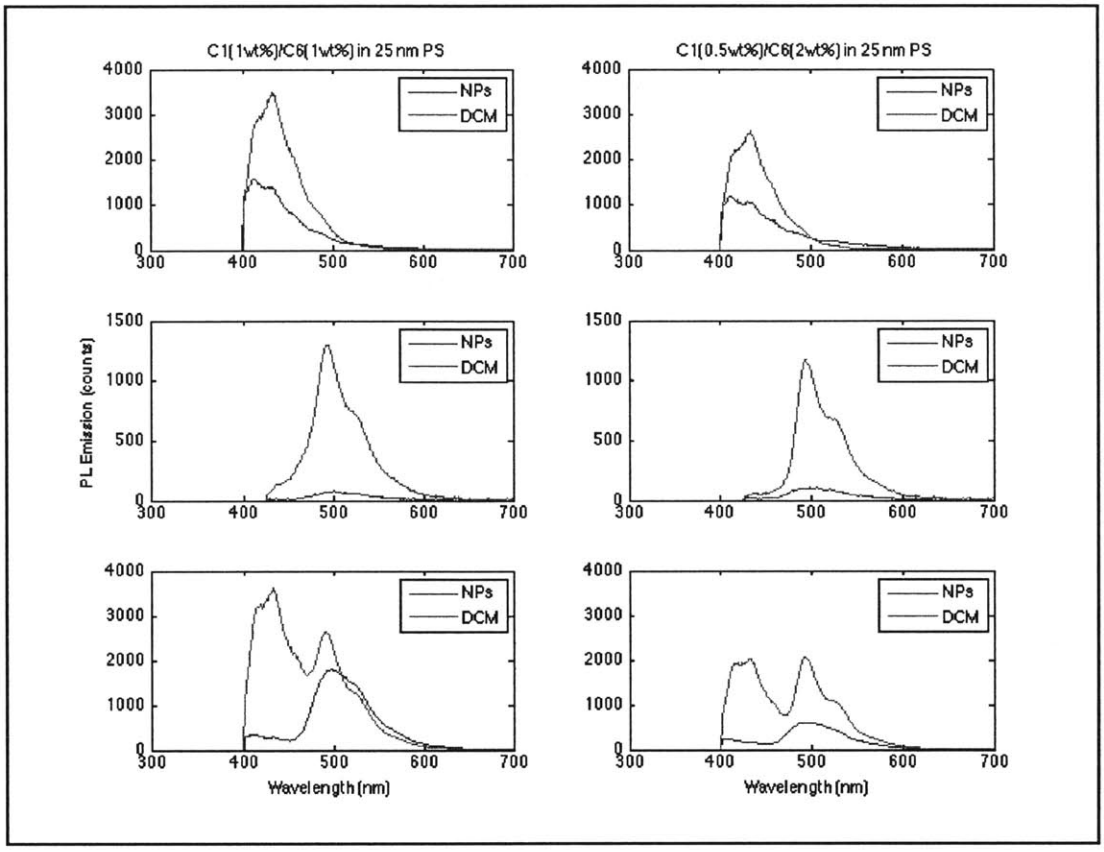

Figure 15: PL emission of C1, C6, and C1/C6 doped nanoparticles in aqueous solution, relative to a DCM control.

The total PL efficiency of the dye-doped nanoparticles was calculated as the ratio of the peak PL intensity of the dye in nanoparticles to that of the control, evaluated at the characteristic peak emission wavelength for that dye:

$$\eta_{PL,NP} = \frac{I_{NP}}{I_{DCM}}$$

Where I_{NP} and I_{DCM} are the PL intensities of the dye in NPs and DCM, respectively, evaluated at the characteristic emission peak of the dye. The resulting total PL efficiencies of the C1 doped nanoparticles and the C6 doped nanoparticles are tabulated below:

Table 1: PL efficiency of the C1-doped nanoparticles and C6-doped nanoparticles

PL efficiencies of C1 nanoparticles and C6 nanoparticles		
	C1(1wt%)/C6(1wt%) iteration	**C1(0.5wt%)/C6(2wt %) iteration**
C1 NP η_{PL}	0.4548	0.4527
C6 NP η_{PL}	0.0646	0.0961

As evident in Table 1, the C6 nanoparticles performed much worse than the C1 nanoparticles. This suggests that either the PL efficiency of C6 in polystyrene is relatively worse, or that the dye-uptake efficiency of C6 during the solvent-evaporation approach is worse – or a combination of both. Notably, during the solvent evaporation approach, it was evident that that a significant fraction of C6 was left in the form of aggregates in solution, and subsequently filtered out. It was unclear by observation whether or not the dye-uptake efficiency was similarly poor for C1, because C1 is colorless in solution.

Importantly, the PL efficiencies of the dye-doped nanoparticles were not dependent on the doping concentrations, which varied from the first iteration to the second. This suggests that either the increased concentration of the starting dye solution did not yield an effective increase in the concentration of dye in the nanoparticles or that the PL efficiency of the dye decreased upon a higher dye concentration in the

nanoparticle. The subsequent calculation of the dye uptake efficiency was therefore critical in determining the correct explanation.

In order to determine the PL efficiency of the dyes in the nanoparticles, the dye uptake efficiency had to also be calculated. In Figure 16, absorbance spectra of the dyes in the nanoparticles were collected with respect to the DCM control:

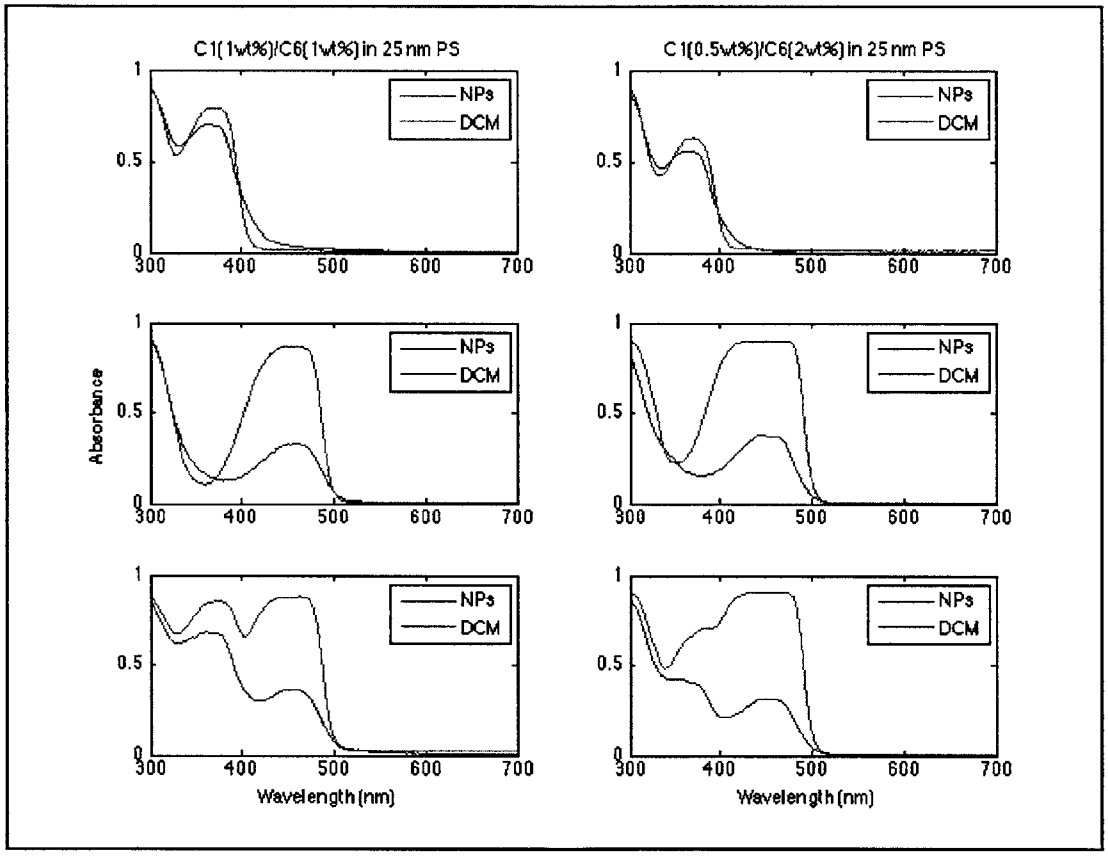

Figure 16: Absorbance spectra of C1, C6, and C1/C6 doped nanoparticles in aqueous solution, relative to the DCM control.

Ideally, if the solvent-evaporation approach were 100% efficient, the two graphs would match up exactly – but this not the case. The dye-uptake efficiency for each dye in the nanoparticles was then calculated using the Beer-Lambert law, which states:

$$A = \varepsilon * b * c$$

Where A is the absorbance of the sample, ε is the molar absorptivity, b is the optical path length and c is the concentration of the solution. Given that the same cuvette models were used for the control solution and nanoparticle solutions, the same optical path length was assumed the same. In addition, it was assumed that molar absorptivity of the dyes in DCM and in the NPs were relatively the same, leading to the following result:

$$\frac{A_{NP}}{A_{DCM}} = \frac{c_{NP}}{c_{DCM}}$$

The above result is the dye-uptake efficiency, a measure of what fraction of the dye from the starting solution effectively diffused into the polystyrene nanoparticles. Thus the dye uptake efficiencies can be calculated by taking the ratio of the peak absorbance of the nanoparticle solutions at the characteristic absorption peak of the dye, with respect to that of the DCM solution:

$$\eta_{uptake} = \frac{A_{NP}}{A_{DCM}}$$

The total dye uptake efficiencies of the C1 doped nanoparticles and the C6 doped nanoparticles are tabulated below:

Table 2: Dye uptake efficiencies of C1 and C6 into the PS nanoparticles after swelling-evaporation

Dye uptake efficiencies of C1 and C6 into PS		
	C1(1wt%)/C6(1wt%) iteration	**C1(0.5wt%)/C6(2wt %) iteration**
C1 NP η_{uptake}	0.881	0.8837
C6 NP η_{uptake}	0.3798	0.4232

As evident in Table 2, the uptake efficiency of C6 was 42% and 47% worse than that of C1 in the first and second iterations, respectively. The data about poor C6 doping therefore corroborates the observation of C6 precipitation and aggregation after the swelling-evaporation procedure was completed. It also suggests that the DCM/PS/Water system may be unfavorable for efficient C6 doping, most likely due to a smaller difference between the solubility of C6 in polystyrene and in water. With a smaller relative solubility difference, there would be a smaller driving force for C6 incorporation into the nanoparticles. For future optimization of the C1 and C6 system, it would be favorable to explore different starting solvents for the dyes and the nanoparticles, as well as different nanoparticle polymer types so as to optimize for effective C1 and C6 doping.

Notably, the dye-uptake efficiency does not change significantly with the doping percentage. In the case of C1, for example, a two-fold decrease in the doping percentage from the first to the second iteration made nearly no measurable effect on the dye-uptake efficiency. While there was a small change for C6, it is similarly negligible.

From the information in Table 1 and Table 2, it is now possible to determine the PL efficiency of the dyes in the nanoparticles. The PL efficiency of C1 and C6 in Polystyrene for each iteration can be summarized below:

Table 3: PL efficiencies of C1 and C6 in Polystyrene

PL efficiencies of C1 and C6 in PS		
	C1(1wt%)/C6(1wt%) iteration	**C1(0.5wt%)/C6(2wt %) iteration**
C1 η_{PL}	0.516	0.512
C6 η_{PL}	0.171	0.227

The results indicate that the PL efficiencies of both dyes in polystyrene were quite low in both iterations. C6 in particular has a very low PL efficiency in polystyrene, further suggesting the proposed system is unfavorable for both effective C6 dye incorporation *and* optical performance. In addition, it also suggests that the reason why C6 dye-uptake is so low may be because C6 does not prefer to be in a polystyrene environment – therefore resulting in a smaller driving force for effective C6 incorporation into the nanoparticles and a reduced PL efficiency. Regardless, the fact that the results indicate the poor performance of both dyes in polystyrene suggests that further exploration of polymer nanoparticle hosts is necessary.

C.) Energy transfer efficiency of C1/C6 dye-doped nanoparticles in liquid PVA

Prior to measuring the energy transfer efficiency of the dye-doped nanoparticles into solid state PVA, we wanted to verify that energy transfer was still occurring even in liquid PVA at increasing dilution of the nanoparticles. If the nanoparticles were to stay in tact and the dyes were to remain together inside, then successive dilutions should have no effect on the energy transfer efficiency, aside from a minimal decrease in self-absorption effects. Given that PS-PVA interactions could yield conformational changes of the nanoparticles, such as swelling, however, this step was important in verifying whether or not the nanoparticles continued to make use of energy transfer upon addition to PVA. A summary of the PL emission data can be found in Figure 17:

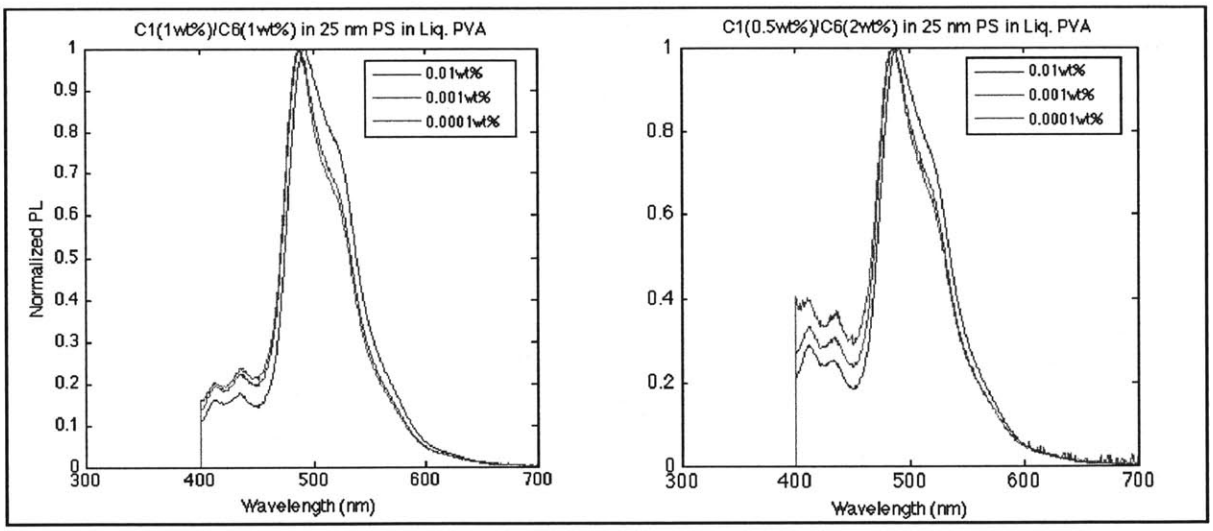

Figure 17: Normalized PL emission spectra of C1/C6 doped nanoparticles in liquid PVA solution at 0.01wt% dye, 0.001wt%dye, and 0.0001wt% dye.

The energy transfer efficiencies were similarly calculated as before, and summarized in the Table 4 below:

Table 4: Energy transfer efficiencies of C1/C6 doped nanoparticles in liquid PVA

Energy transfer efficiencies of C1/ C6 in PS in liquid PVA		
	C1(1wt%)/C6(1wt%) iteration	**C1(0.5wt%)/C6(2wt %) iteration**
0.01wt% dye	0.823	0.713
0.001wt% dye	0.777	0.668
0.0001wt% dye	0.727	0.623

For the first iteration nanoparticles, the energy transfer efficiency remains relatively unchanged for all samples, however there is a slight decrease in the energy transfer efficiency of about 10% as the total weight percentage of dye in PVA decreases. In the end, the energy transfer efficiency saturates at around 73%. This suggests that the nanoparticles remain relatively in tact and continue to make use of energy transfer, but the decrease in energy transfer efficiency is a result of both decreased self-quenching effects at higher dilutions and possibly minimal diffusion of the dye molecules into PVA.

While the second iteration nanoparticles similarly have a 9% reduction in energy transfer efficiency over the successive dilutions, there does not seem to be saturation energy transfer efficiency. This suggests that the actual energy transfer efficiency of the second iteration nanoparticles may be even lower than the 0.0001wt% sample, since as the affects of self-absorption become more and more negligible, the energy transfer efficiency is revealed to be lower and lower. Regardless, however, even at extremely low wt% dye doping, there is significant energy transfer in both iterations.

D.) Energy transfer efficiency of C1/C6 dye-doped nanoparticles in liquid PVA

In the final step of the process, the dye-doped nanoparticles in liquid PVA solution were drop casted onto a glass slide. As mentioned before, the energy transfer efficiency should theoretically have remained relatively constant (neglecting any minimal self-absorption effects), assuming that the dyes remain embedded in the nanospheres and the nanospheres retains its size and shape. The PL emission data of the solid-state samples was plotted in Figure 18:

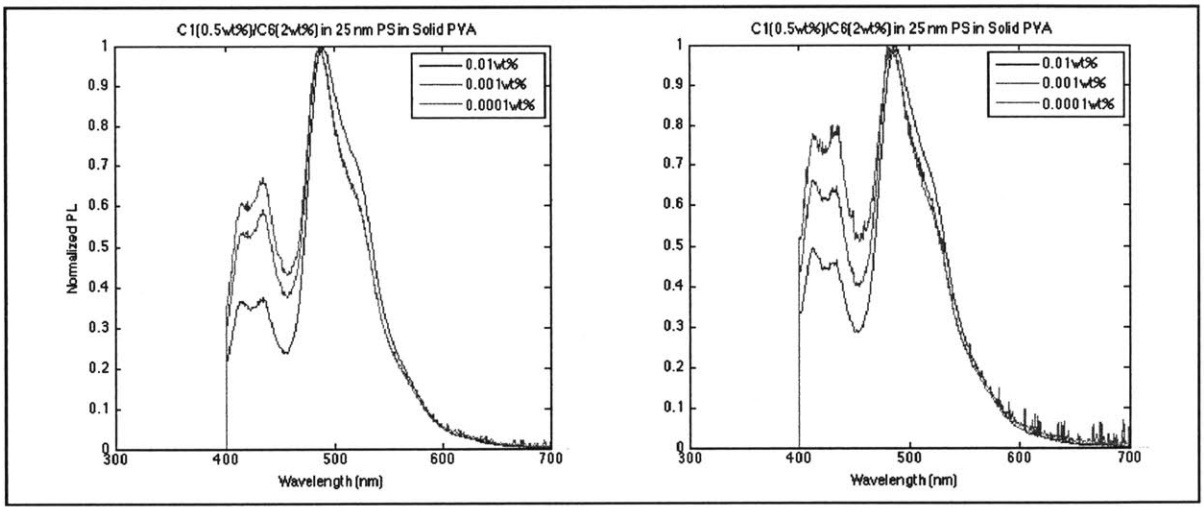

Figure 18: Normalized PL emission spectra of C1/C6 doped nanoparticles in solid state PVA at 0.01wt% dye, 0.001wt%dye, and 0.0001wt% dye.

The energy transfer efficiencies were similarly calculated as before, and summarized in the Table 5:

Table 5: Energy transfer efficiencies of C1/C6 doped nanoparticles in solid state PVA

Energy transfer efficiencies of C1/ C6 in PS in solid PVA		
	C1(1wt%)/C6(1wt%) iteration	**C1(0.5wt%)/C6(2wt %) iteration**
0.01wt% dye	0.627	0.504
0.001wt% dye	0.411	0.334
0.0001wt% dye	0.328	0.201

As evident by the graph, the PL spectra of both iterations become increasingly more C1-like, suggesting a drop in energy transfer efficiency. Table 5 meanwhile indicates that the energy transfer efficiency of the both iterations drops 30% after 100x dilution. Just like in the liquid PVA case, the first iteration nanoparticles present a saturation trend, whereas the second iteration nanoparticles do not. Similarly, this suggests that the actual energy transfer efficiency of the second iteration solution may be even less than that measured for the 0.0001wt% solution.

Notably, the energy transfer efficiencies of all the solid PVA samples were smaller than those of the liquid PVA samples, suggesting that dye was further leaching out of the nanoparticles during the PVA drying phase. To that end, it may be likely that the dyes were situated at the outermost part of the nanospheres, and upon water evaporation, dye diffusion into PVA increased. It remains unclear whether or not the dyes were diffusing in the solid state into the PVA or with the mobile water phase that was evaporating. However, given the hydrophobic properties of the dyes, it is likely that the dyes preferentially diffuse into PVA in the solid state. Importantly, since energy transfer efficiency is so sensitive to the radius, even a very small diffusion of dyes out of the nanoparticles could yield a significant loss in the energy transfer efficiency.

E.) Absorbance of C1/C6 dye-doped nanoparticles in solid state PVA

One of the important characteristics of an LSC is transparency. To that end, we wanted to verify whether or not PVA was a successful matrix in terms of creating uniform, non-scattering solid-state samples. A summary of the Aquila absorbance data can be found in Figures 19 and 20:

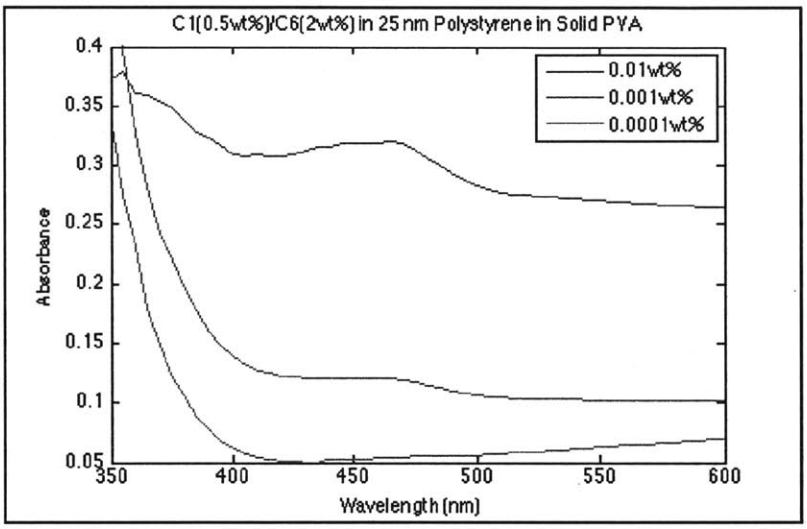

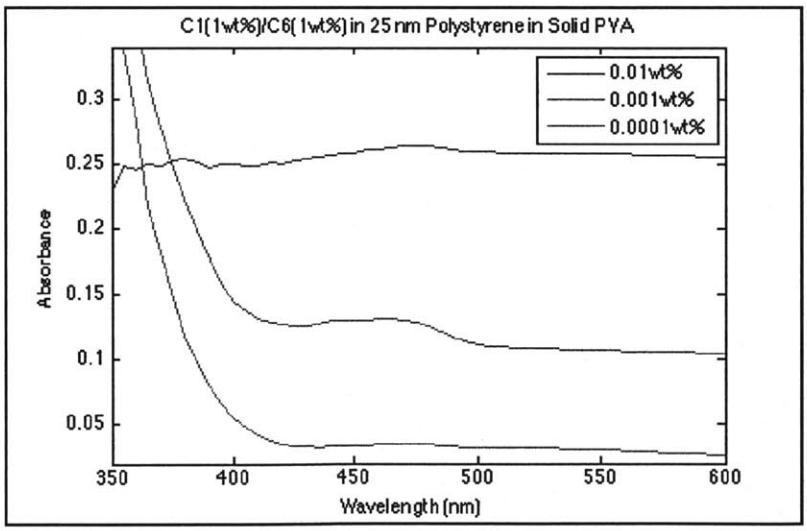

Figures 19 and 20: Absorbance of solid state C1/C7 doped nanoparticles in PVA at different total wt% of dye for C1(1wt%)/C6(1wt%) model (bottom) and C1(0.5wt%)/C6(2wt%) model (top).

As expected, Figures 19 and 20 demonstrate the absorbance of the samples across the visible spectrum decreases with increasing dilution. For the first iteration of nanoparticles, the absorbance decreases from near 26% at 0.01wt% dye to approximately 3% for the 0.0001wt% solutions. Meanwhile, for the second iteration of nanoparticles, the absorbance decreases from near 30% at 0.01wt% dye to approximately 6% for the 0.0001wt% solutions. Thus, at lower and lower effective dye concentrations, the solid state samples become less and less absorbent – and consequentially more transparent.

Notably, the C1 and C6 peaks are still noticeable at such high dilutions. For the 0.01wt% the peaks are especially noticeable, suggesting that C1 and C6 are in fact still inside the LSC – though this is expected since it would be highly unlikely for the dyes to evaporate out of the PVA film. Importantly, however, the C1 peaks are especially undetermined at higher dilutions. This is most likely because the Aquila Tungsten lamp is only rated to 400 nm, and because lensing effects of the solid state LSCs could have disrupted the signal.

In total, the relatively low overall magnitude of the absorbance for the solid-state samples suggests that the solid-state samples are transparent and that index matching is occurring. As theoretically predicted, the index matching of PVA to PS did in fact lead to a transparent bulk LSC.

CONCLUSION

The preliminary goal of this thesis was to realize a solid state LSC comprised of dye-doped nanoparticles. To that end, C1/C6 doped nanoparticles were incorporated into a solid state LSC with a maximal energy transfer efficiency of 62% for C1(1wt%)/C6(1wt%) doped nanoparticles diluted in PVA to 0.01 total wt% dye. However, the actual energy transfer efficiency of the dye-doped nanoparticles was most likely lower, given that the energy transfer efficiency decreased to a minimum of 32.8% and 20.1% respectively for the C1(1wt%)/C6(1wt%) and C1(0.5wt%)/C6(1wt%) iterations upon increased nanoparticle dilution in PVA. This suggests that dye confinement is lost in the solid state, most likely due to diffusion of the dyes out of the nanoparticles upon addition to liquid PVA, and further diffusion into PVA upon water evaporation.

Although the preliminary goal of this thesis was not met, C1 and C6 were indeed doped into the polystyrene nanoparticles and showed excellent maximal energy transfer of 87% for the C1(1wt%)/C6(1wt%) aqueous nanoparticle solutions. In addition, the PVA matrix was proven to be an effective host for polystyrene nanoparticles because it made a transparent LSC, void of scattering.

Future work will be focused on first verifying the mechanism leading to the loss of dye-confinement in the solid state. To that end, fluorescence microscopy measurements could be used to determine the locations of the dyes post-drop casting – and by extension, whether or not the dyes are diffusing into the PVA. TEM studies could also verify whether or not the nanoparticles were swelling in PVA, thereby increasing the effective spacing between dye molecules and decreasing the likelihood of FRET. In addition,

future work should identify whether or not the dyes are diffusing with the mobile phase of water upon evaporation out of the dye.

Once this loss mechanism is identified, subsequent work could focus on finding a suitable system that supports energy transfer of the dye-doped nanoparticles in the solid state LSC. This work would require optimizing many parameters – such as nanoparticle polymer choice, solvent choice, matrix choice, or swelling procedure. An optimal procedure would ensure high dye-uptake efficiencies of the donor and acceptor, high PL efficiency of the dyes in the nanoparticles, high energy transfer efficiency, and a high transparency. Once this process is determined, the ultimate goal of this thesis will be realized.

BIBLIOGRAPHY

1. Interstate Renewable Energy Council. *United States Solar Market Trends, 2010.*
2. United States Department of Energy, Energy Efficiency and Renewable Energy. *Photovoltaics Subprogram*, 2009.
3. Timilsina, Govina et al. "Solar energy: markets, economics, and policies." *Renewable and Sustainable Energy Reviews* 16 (2012). 449-465..
4. Van Sark, Wilfried. "Luminescent solar concentrators: A low cost photovoltaic alternative." *Renewable Energy* 49 (2013). 207-210.
5. Baldo, Marc, et al. "High-efficiency organic solar concentrators for photovoltaics." *Science* 321 (2008). 226–228.
6. Buonassisi, Tonio. "Costs prices and markets (part 1)." Fundamentals of photovoltaics, 2010, Lecture.
7. Mulder, Carlijn L. "Engineering the optical properties of luminescent solar concentrators at the molecular scale". Diss. Massachusetts Institute of Technology, Dept. of Electrical Engineering and Computer Science, 2012. *Dissertations and Theses*. Web 15 Feb 2013.
8. Buonassisi, Tonio. "Costs prices and markets (part 2)." Fundamentals of photovoltaics, 2010, Lecture.
9. Mills, David, et al. "Cooling of photovoltaic cells under concentrated illumination: a critical review". *Solar Energy Materials and Solar Cells* 86.4 (2005). 451–483.
10. Koole, et al. "Fabrication and full characterization of state-of-the-art quantum dot luminescent solar concentrators".*Solar Energy Materials and Solar Cells,* 95, 8 (2011), pp 2087-2094.

11. W.H. Weber, J. Lambe, "Luminescent greenhouse collector for solar radiation", *Applied Optics*, 15 (1976), pp. 2299–2300.

12. Richards, et al. "Advanced material concepts for luminescent solar concentrators", *IEEE Journal of Selected Topics in Quantum Electronics* ,14 (2008), pp. 1312–1322.

13. R. Reisfeld. "Prospects of sol-gel technology towards luminescent materials", *Optical Materials*, 16 (2001), pp. 1–7.

14. P.C. Eames, et al. "Quantum dot solar concentrators: electrical conversion efficiencies and comparative concentrating factors of fabricated devices", *Solar Energy*, 81 (2007), pp. 813–821.

15. Carter, et al. "Optimization of gain and energy conversion efficiency using front-facing photovoltaic cell luminescent solar concentrator design." *Solar Energy Materials and Solar Cells*, 111 (2013), pp. 74-81.

16. Baldo et al. "High-efficiency organic solar concentrators for photovoltaics." *Science*, 321 (2008), pp. 226–228

17. Richards et al. "Enhancing the performance of solar cells via luminescent down-shifting of the incident spectrum: A review." *Solar Energy Materials and Solar Cells*, 83 (2009), pp. 1182-1194.

18. Bates, Seth. "Silicon wafer processing." Applied Materials, 2000, Lecture.

19. Fresnel Equations. *Microoptics Laboratory – Department of Hanyang University*. Web 10 Feb. 2013.

20. Barnham, K.W.J, et al. "Luminescent Solar Concentrators: Cylindrical Design." 24th European Photovoltaic Solar Energy Conference, 21-25 September 2009, Hamburg, Germany.

21. Yablonovitch, et al. "The Thermodynamic Limits of Light Concentrators". *Solar Energy Materials* 21 (1990). 99-111.

22. Fresnel Equations. *Microoptics Laboratory – Department of Hanyang University.* Web 10 Feb. 2013.

23. Ram, Rajeev. "Polarizers and Polarization" Electromagnetic Energy: From Motors to Lasers, 2013, Lecture.

24. Rüdiger Sens, Karl H. Drexhage. "Flourescence quantum yield of oxazine and carbazine laser dyes." *Journal of Luminescence* 24 (1981). 709-712

25. Drexhage, Karl. H. "Flouresence efficiency of laser dyes." *Advanced Physics and Chemistry* 80A (1976). 421-428.

26. Currie, Michael J. "Fabrication of LSC that Minimizes Self-Absorption". MA Thesis, Masschusetts Intitute of Technology, 2007. *Dissertations and Thesis.* Web 22 Feb. 2013.

27. Debije, Michael, et al. "Influence of waveguide material on light emission in luminescent solar concentrators." *Optical Materials* 31.11 (2009). 1720-1722.

28. Wittmer- shaus, B.P, et al. "Optimized excitation energy transfer in a three-dye luminescent solar concentrator." *Solar Energy Materials and Solar Cells,* 91.1 (2009). 67-

29. Wilson, Lindsay R. "A study of optical properties, re-absorption, and device optimization". Diss. Heriot Watt University, 2010. *Dissertations and Thesis.* 19 Feb 2013.

30. McNeill, Jason, et al. "Energy Transfer in a nanoscale multichromophoric system: fluorescent dye-doped conjugated polymer nanoparticles." *J. Phys. Chem. C 112.*6 (2008).1772–1781.

31. Forster, Disc. Laboratory of Physical Chemistry, Technische Hochschule, Stuttgart, 10th Spiers Memorial Lecture, "Transfer Mechanisms of Electronic Excitation", Apr. 14, 1959

32. Rowan, Brendan C., Wilson, Lindsay, and Richards, Bryce. "Advanced material concepts for luminescent solar concentrators." *IEEE Journal of Selected Topics in Quantum Electroncis* 14.5 (2008). 1312-1322.

33. Tan, Weihong, et al. "Doped nanoparticles for bio-analysis." *Nanotoday* June 2007. 44-50.

34. Chen, S, et al. "Fluorescence resonance energy transfer mediated large Stokes shifting near-infrared fluorescent silica nanoparticles for in vivo small-animal imaging." *Analytical Chemistry* 84.21 (2012). 9056-9064.

35. Li, Ming, Rouand, Oliver, and Poncelet, Denis. "Microencapsulation by solvent evaporation: State of the art for process." *International Journal of Pharmaceuticals* 363.1 (2007). 26-39.

37. Wu, Changfeng and McNeill, Jason. "Swelling-controlled polymer phase and fluorescence properties of polyfluorene nanoparticles."

38. Zeilder, Anita, et al. "Molecular origins of optoelectronicp in coumarin dyes: toward designer solar cell and laser applications." *Journal of Physical Chemistry* 116.1. 727-737.

39. Senthikumar, S., Nath, Sukhendu, and Haridas Pal. "Photophysical properties of coumarin-30 dye in aprotic and protic solvents of varying polarities". *Photochemistry and Photobiology* 80.1 (2004). 104-11.

40. "Plastics". *Refractive Index Informartion.* Web. Jan. 26, 2013.

41. "Examples of Embedding Media." *Scientific Volume Imaging.* Web. Feb. 6, 2013.

42. "Mowiol." *Kurary.* Web. Feb. 25, 2013.

43. "Coumarin 1". *Oregon Medical Laser Center.* Web. Mar. 1, 2013.